# Probing the Distribution of Water Molecules Hydrating Lipid Membranes with Ultrafast Förster Vibrational Energy Transfer

L. Piatkowski,* J. de Heij, and Huib J. Bakker

FOM Institute AMOLF, Science Park 104, 1098 XG Amsterdam, The Netherlands

ABSTRACT: We determine the relative positioning of water molecules in 1,2-dioleoyl-*sn*-glycero-3-phosphocholine (DOPC) membranes by measuring the rate of vibrational resonant (Förster) energy transfer between the water hydroxyl stretch vibrations. The rate of Förster energy transfer is strongly distance dependent and thus gives detailed information on the relative positioning of the water molecules. We determine the rate of intermolecular Förster energy by measuring the anisotropy dynamics of excited O−D stretch vibrations of HDO and D_2O molecules with polarization-resolved femtosecond mid-infrared spectroscopy. We study the dynamics for deuterium fractions between 0.1 and 1 and for hydration levels between 2 and 12 water molecules per DOPC lipid molecule. We find that most of the water molecules hydrating the membrane are contained in nanoclusters and have an average intermolecular distance of 3.4 Å. The density of these nanoclusters increases with increasing hydration level of the DOPC membranes.
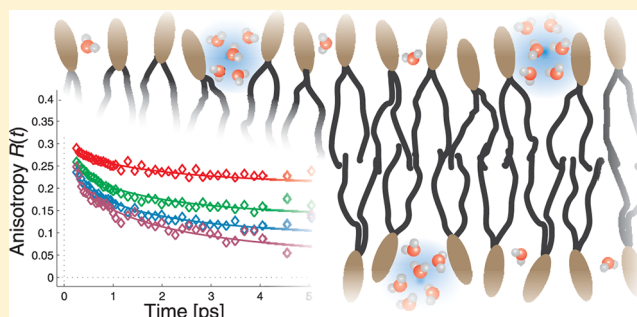
INTRODUCTION

Water plays a crucial role in the self-organized formation of cell membranes and in most of their transport and signaling functions.[1] To acquire a better understanding of this role of water, the structure and dynamics of water hydrating phospholipid membranes have been studied intensively using NMR,[2,3] infrared spectroscopy,[4−6] molecular dynamics simulations,[7−12] nonlinear spectroscopy,[13−17,19−21] and dielectric relaxation spectroscopy.[22,23]

In many studies it is found that the water molecules hydrating a phospholipid membrane show a large variety in hydrogen-bond strength[4−21] and that part of the water molecules forms quite strong hydrogen bonds with the headgroup of the phospholipid molecule, in particular with the phosphate group. Two-dimensional femtosecond vibrational spectroscopic studies of water hydrating 1-palmitoyl-2-linoleylphosphatidycholine (PLPC)[16] and dimyristoylphosphatidylcholine (DMPC)[18] showed that the water molecules can be doubly hydrogen bonded, singly hydrogen bonded, and even non-hydrogen bonded. For the singly hydrogen bonded species one of the O−H groups is (strongly) hydrogen bonded to the phospholipid while the other O−H groups is a dangling O−H group.

The water molecules hydrating a lipid membrane show a large variation in the rate of vibrational energy relaxation.[17,21] For water molecules hydrating dilauroylphosphatidylcholine (DLPC), the observed variation in the vibrational lifetime was explained from the presence of two different water molecules: water molecules that are bound to the phosphate group and water molecules that are associated with the choline group of the lipid.[17] At present there is quite some knowledge on the local binding and energy dynamics of water molecules

hydrating the head groups of phospholipids. However, not much is known on the positions of the water molecules with respect to each other and the phospholipids.

Here we report on the use of resonant (Förster) vibrational energy transfer as a new method to determine the relative positions of water molecules hydrating a bilayer of 1,2-dioleoyl-*sn*-glycero-3-phosphocholine (DOPC) lipids. The rate of Förster energy transfer strongly depends on the distance between donating and accepting resonances and can thus be used as a subnanometer ruler. Förster energy transfer is a common phenomenon for electronic excitations and is widely used to determine the distance between chromophoric (dye) molecules.[24−27] For molecular vibrations, Förster energy transfer is much less common, due to the relatively small transition dipole moment of molecular vibrations and the short subpicosecond to picosecond lifetime of vibrational excitations in the condensed phase.

We measure the rate of Förster vibrational energy transfer between hydrating water molecules with polarization-resolved ultrafast pump−probe spectroscopy. In this technique we make use of the fact that the resonant energy transfer between the hydroxyl vibrations of the water molecules leads to a depolarization of the vibrational excitation. This technique has been used before to measure the rate of Förster vibrational energy transfer for different isotopic compositions of neat water.[28−32] These studies gave information on the strength of the dipolar coupling between the O−H/O−D stretch vibrations located on different water molecules. Here we

show that for hydrated systems the rate of intermolecular Förster vibrational energy transfer provides important information on the amount of clustering of the water molecules.

THEORY

Resonant (Förster) energy transfer results from the dipole–dipole coupling between an excited donor molecule and an unexcited acceptor molecule. In the original expression derived by Förster, all possible donor–acceptor interactions are included assuming that the acceptors are statistically distributed.[33] For a system like liquid water, energy transfer between the hydroxyl stretch vibration can take place both within the molecule and between different molecules. The Förster expression does not make a distinction between these two types of energy transfer. To use Förster energy transfer as a method to determine the distance between water molecules, the intramolecular contribution should be removed from the Förster expression. Here we derive such a modified expression. The contribution of the intramolecular energy transfer will be described in a separate expression in which obviously the distance between different water molecules does not play a role.

The rate constant of Förster energy transfer k_F is given by[24,33]

$$k_{F,ab} \propto \frac{|\vec{\mu}_a|^2 |\vec{\mu}_b|^2 \kappa_{ab}^2}{|\vec{R}_{ab}|^6} \int d\nu \, \sigma_a(\nu) \, \sigma_b(\nu) \quad (1)$$

where $\vec{\mu}_a$ and $\vec{\mu}_b$ are the vibrational transition dipole moments of the donating and accepting oscillators, κ_{ab} is a geometrical factor taking into account the mutual orientation of the oscillators, and R_{ab} is the distance between the two molecules. The integral evaluates the spectral overlap between the emission and absorption spectra of the donor and acceptor.

If we assume that the orientation between the dipoles is independent of the distance R_{ab}, we can express the Förster transfer rate as

$$k_j = \frac{1}{T_1} \left(\frac{r_0}{r_j} \right)^6 \quad (2)$$

where T_1 is the intrinsic lifetime of the excitation in the absence of the energy transfer and r_0 is the so-called Förster radius. It follows from eq 1 that the Förster rate depends on the transition dipole moments of the donor and acceptor, the homogeneous line shapes, and the relative orientation of the donors and acceptors. These parameters are collectively represented by $r_0^6 t / T_1$, meaning that the value of the Förster radius r_0 is defined as the distance between donor and acceptor for which energy transfer occurs with 50% probability within the lifetime T_1 of the excitation.

The probability that an excited molecule remains excited at time $t = \tau$ is

$$\rho(\tau) = \prod_{j=1}^{N_{OD}} \exp(-k_j \tau) \quad (3)$$

where N_{OD} is the number of accepting oscillators and k_j is the rate constant for energy transfer to that oscillator. The probability to find an accepting molecule at a distance between r_j and $r_j + dr_j$ is equal to the volume of the spherical shell normalized to the total volume of the sample V

$$\eta(r) = \frac{4\pi r_j^2 \, dr_j}{V} \qquad \text{where} \quad V = \frac{4\pi R^3}{3} \quad (4)$$

with R the radius of the sphere. Substituting eq 2 in eq 3 and integrating over all possible acceptors we arrive at

$$\rho(t) = \left\{ \frac{4\pi}{V} \int_0^R \exp\left(-\frac{t r_0^6}{T_1 r^6} \right) r^2 \, dr \right\}^{N_{OD}} \quad (5)$$

This approach assumes a statistical distribution of molecules, and the integral is usually performed with $r = 0$ as a lower boundary. In the case of energy transfer between the hydroxyl vibrations of water molecules, it thus intrinsically takes into account intramolecular energy transfer processes between the two hydroxyl stretch vibrations of a water molecule. We remove the intramolecular contribution from the Förster expression by starting the integration from a distance $r = a$, which should be larger than the intramolecular distance between the hydroxyl groups ~1.55 Å) but shorter than the minimal intermolecular distance between water molecules (~2.2 Å). The excitation survival probability $\rho(t)$ is thus given by

$$\rho(t) = \left\{ \frac{4\pi}{V} \int_a^R \exp\left(\frac{-t r_0^6}{T_1 r^6} \right) r^2 \, dr \right\}^{N_{OD}} \quad (6)$$

Performing the integration, we obtain

$$\rho(t) = \left\{ \exp\left(-\frac{t r_0^6}{T_1 R^6} \right) - \frac{a^3}{R^3} \exp\left(-\frac{t r_0^6}{T_1 a^6} \right) \right.$$
$$\left. + \sqrt{\frac{\pi t r_0^6}{T_1 R^6}} \, \text{erf}\left(\sqrt{\frac{t r_0^6}{T_1 R^6}} \right) - \sqrt{\frac{\pi t r_0^6}{T_1 R^6}} \, \text{erf}\left(\sqrt{\frac{t r_0^6}{T_1 a^6}} \right) \right\}^{N_{OD}} \quad (7)$$

The concentration C_{OD} of O–D oscillators is $C_{OD} = 3N_{OD}/4\pi R^3$ [expressed in (molecules/Å^3)]. Using this expression we can eliminate R. Expanding the exponential function and the error function in terms of $1/N_{OD}$ we arrive at

$$\rho(\tau) = \left\{ 1 - \left[\frac{4\pi C_{OD} a^3}{3} \exp\left(-\frac{t r_0^6}{T_1 a^6} \right) + \frac{4\pi^{3/2} C_{OD} r_0^3 \sqrt{t}}{3\sqrt{T_1}} \right. \right.$$
$$\left. \left. \text{erf}\left(\sqrt{\frac{t r_0^6}{T_1 a^6}} \right) \right] \left(\frac{1}{N_{OD}} \right) + \alpha \left(\frac{1}{N_{OD}} \right)^2 \right\}^{N_{OD}} \quad (8)$$

The number of accepting molecules is in most cases very large, so the terms proportional to $(1/N_{OD})^2$ become small and can be neglected. In that case, the above equation can be approximated by

$$\rho(t) = \exp\left\{ -\frac{4\pi C_{OD} a^3}{3} \exp\left(-\frac{t r_0^6}{T_1 a^6} \right) - \frac{4\pi^{3/2} C_{OD} r_0^3 \sqrt{t}}{3\sqrt{T_1}} \right.$$
$$\left. \text{erf}\left(\sqrt{\frac{t r_0^6}{T_1 a^6}} \right) \right\} \quad (9)$$

For $a \to 0$, the above formula reduces to the well-known Förster expression for the survival probability:[28,32]

$$\rho(t) = \exp\left(-\frac{4\pi^{3/2}C_{OD}r_0^3\sqrt{t}}{3\sqrt{T_1}}\right) \tag{10}$$

Figure 1 shows the time dependence of $\rho(t)$ calculated with eq 9 for different values of a. It is clearly seen that the decay of
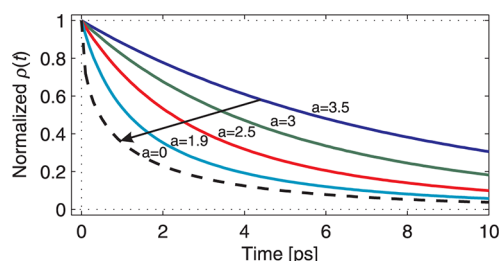
Figure 1. Excitation survival probability function for various minimal energy transfer distances a.

$\rho(t)$ slows down with increasing value of a, especially at short delay times. This can be understood from the fact that the contribution of the fast donor–acceptor pairs, for which the mutual distance is smaller than a, has been removed.

■ EXPERIMENTAL SECTION

We studied the energy transfer dynamics of water molecules hydrating DOPC membranes with polarization-resolved femtosecond pump–probe spectroscopy. The laser system used for these experiments generates pulses at a wavelength of 800 nm with a pulse energy of ~900 μJ at a repetition rate of 1 kHz. The 800 nm pulses are split into two parts of which the first part (~600 μJ) is used to pump a white-light based Optical Parametric Amplifier (OPA) (Spectra Physics). After the OPA the idler is frequency doubled in a second BBO crystal. The doubled idler (1000 nm) is used as a seed in a parametric amplification process in a potassium niobate crystal (KNB), pumped with the remaining ~300 μJ of the 800 nm pulse. The generated femtosecond infrared laser pulses have a pulse duration of ~100 fs, a tunable center wavelength near 4 μm (~2500 cm^{-1}), and a pulse energy of ~6 μJ.

The mid-infrared pulses are used in a polarization-resolved pump–probe experiment on the O–D stretch vibration of HDO and D$_2$O molecules. The probe pulse is split off from the infrared pulses using a wedged CaF$_2$ plate. The transmitted part (92%) is used as the pump. The reflection from the front side (4%) is sent into a delay stage to vary the time delay between the pump and probe pulses. The pump and probe are focused to the same spot in the sample using a gold-coated parabolic mirror. The reflection from the back side of the wedged CaF$_2$ plate (4%) is also focused in the sample by the same mirror, but not in overlap with the pump. This beam is used as a reference. The pump promotes population from the equilibrium ground-state $v = 0$ of the O–D stretch vibrations of HDO and D$_2$O to the first excited state, $v = 1$. This excitation is observed as a bleach and stimulated emission at frequencies matching $v = 0 \rightarrow 1$ and an induced absorption at frequencies matching $v = 1 \rightarrow 2$. After the sample, the probe and reference are dispersed with an Oriel monochromator and detected with the two lines of an Infrared Associates 2×32 MCT (mercury–cadmium–telluride) detector array. The measurement of the reference allows for a frequency-resolved correction of the shot-to-shot fluctuations of the probe–pulse energy.

We measure the pump-induced frequency-resolved transient absorption spectra as a function of time delay between pump and probe. Before entering the sample, the polarization of the probe is rotated at 45° with respect to the pump polarization using a half-wave plate. After the sample the polarization component parallel to the pump or the component perpendicular to the pump is selected using a polarizer mounted in a motorized rotation stage. The thus obtained transient absorption changes $\Delta\alpha_\parallel(t)$ and $\Delta\alpha_\perp(t)$ are used to construct the anisotropy parameter $R(t)$:

$$R(t) = \frac{\Delta\alpha_\parallel(t) - \Delta\alpha_\perp(t)}{\Delta\alpha_\parallel(t) + 2\Delta\alpha_\perp(t)} \tag{11}$$

The denominator of $R(t)$, $\Delta\alpha_\parallel(t) + 2\Delta\alpha_\perp(t)$, constitutes the isotropic signal. $R(t)$ represents the normalized difference between the signals measured with parallel and perpendicular pump–probe polarizations and is thus insensitive to vibrational relaxation. $R(t)$ only decays as a result of molecular reorientation and resonant Förster energy transfer between differently oriented O–D stretch vibrations of donor and acceptor HDO and D$_2$O molecules.

We obtained DOPC from Avanti Polar Lipids and used it without further purification. DOPC is a zwitterionic lipid, carrying positive and negative charges on different atoms of the lipid headgroup. We prepare a stack of solid-supported, oriented DOPC bilayers with a technique adapted from previous reports.[34−38] The dry lipids are dissolved in a methanol/chloroform mixture (1:3 volumetric ratio) at a concentration of 50 g/L. We deposit a small amount of the solution (5−15 μL) on the CaF$_2$ window and wait for a few minutes until the solvent evaporates. We repeat this process until the desired thickness of the sample is achieved. The sample is then placed in a home-built sample holder that is sealed from the environment. We dry the sample by purging nitrogen gas through the sample holder.

After drying, the samples are equilibrated with air of a well-defined relative humidity. The samples are hydrated with mixtures of H$_2$O and D$_2$O (Sigma-Aldrich, 99.9% D) with a home-built hydration system that allows for generating air with relative humidities (RH) in the range of 15−95% with a precision of 3%. After the hydration process the sample is put in between two CaF$_2$ windows separated with a Teflon spacer with a thickness in the range from 10 to 150 μm, depending on the hydration level and the isotopic composition of the hydrating water. The final hydration of the samples was checked by comparing the linear absorption spectrum with the absorption spectrum of a reference sample. The reference sample was a diluted, homogeneous solution of DOPC in chloroform to which a well-defined amount of D$_2$O was added, such that a specific water/lipid molecular ratio (1:1, 1:2, 1:4, 1:6, 1:8, and 1:10) is obtained.

Hydrated DOPC arranges in stacked bilayers.[34−42] We align the bilayers by means of a thermal and mechanical sample treatment reported previously.[34−38] Once the sample is hydrated and sealed between the CaF$_2$, we heat the sample cell in the range of 40−80 °C, depending on the thickness and the hydration level, and we move the two windows with respect to each other while gently applying pressure to the sample. The flow of the material resulting from the shear enables the sample to adapt to the energetically favorable stacked planar form.

Following the hydration and alignment procedure, we place every sample in between two orthogonally oriented polarizers
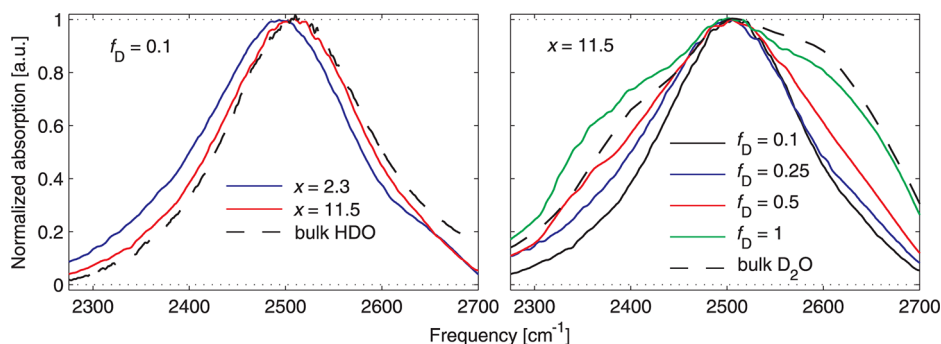
Figure 2. Linear absorption spectra of hydrated lipids in the frequency region of the O−D stretch vibration of HDO and D_2O. The left panel shows the absorption spectra of HDO molecules at a deuterium fraction $f_D = 0.1$ hydrating DOPC for two different hydration levels. For comparison the absorption spectrum of a dilute solution of HDO in H_2O is shown. The right panel shows the absorption spectra of water of different deuterium fractions f_D hydrating DOPC at a hydration level $x = 6.4$. For comparison, the right panel also shows the absorption spectrum of pure D_2O.
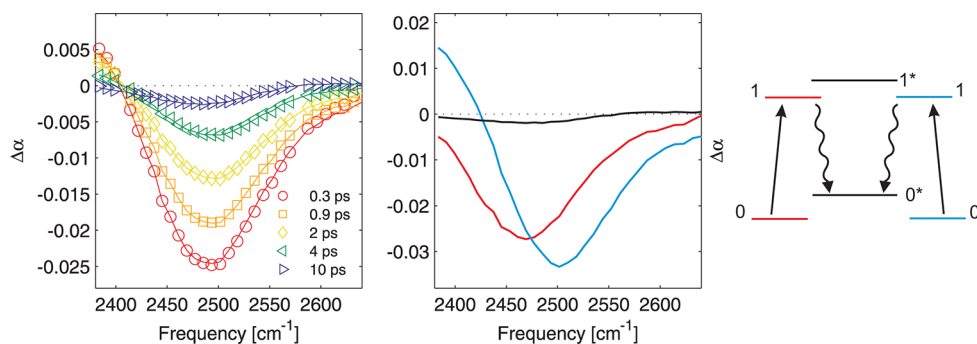
Figure 3. Left panel: difference spectra between the transient absorption spectra measured at different delays after excitation by the pump pulse and the linear absorption spectrum, in the frequency region of the O−D stretch vibration of HDO and D_2O molecules. The spectra are measured for DOPC layers hydrated with 6.4 water molecules per lipid and a deuterium fraction $f_D = 0.1$. Middle panel: spectral components resulting from the decomposition of the difference spectra. The red and blue lines indicate different water species adsorbed to DOPC. The black line is the thermal difference spectrum resulting after the relaxation of the red and blue components. Right panel: vibrational level scheme corresponding to the spectral decomposition.

and we check its transmission under orthoscopic white light illumination with a Nikon Eclipse Ti inverted microscope connected to a Photometrics Coolsnap HQ2 digital CCD camera. Well-aligned, monodomain lipid multilayers appear black when viewed between two crossed polarizers under an orthoscopic white light. After the pump−probe measurements we re-examined each sample. We did not observe any changes in the linear absorption spectrum or the alignment after the femtosecond experiments.

We studied stacked DOPC bilayers at different hydration levels (25%, 50%, 75%, and 100% RH, which correspond to $x = 2.3, 3.5, 6.4,$ and 11.5 water molecules per lipid, respectively). At each hydration level we performed measurement for four different isotopic compositions of water, which we label by the fraction f_D of O−D oscillators: $f_D = 0.1, 0.25, 0.5,$ and 1.

Recently, the isotope effect on the structure and dynamics of lipid membranes has been studied both experimentally and theoretically.[45,46] It is found that the structural and dynamical properties of the membranes themselves are hardly affected by exchanging H_2O by D_2O; typically, the effect is on the order of a few percent. In our experiment, we vary the isotopic composition from 10% D_2O in H_2O to pure D_2O, and we observe no significant change of the vibrational spectrum or other properties of the membrane lipids. Therefore, the variation of the isotope composition allows for an accurate investigation of the structural and dynamical properties of water molecules interacting with the membrane.

RESULTS AND INTERPRETATION

Linear Absorption Spectra. In Figure 2 we show linear absorption spectra in the frequency region of the O−D stretch vibration of HDO and D_2O. The left panel shows that the absorption spectrum of the O−D vibration of the hydrating HDO molecules is red-shifted with respect to the absorption band of HDO dissolved in H_2O, in particular for a low hydration level $x = 2.3$ This red-shift indicates that a significant part of the water molecules forms stronger hydrogen bonds with the DOPC lipid molecules than with other water molecules.[6,17] At a high hydration level $x = 11.5$, the red-shift is much smaller, indicating that at this hydration level most of the HDO molecules are hydrogen bonded to other water molecules. In the right panel we compare the absorption spectrum of water hydrating DOPC for different deuterium fractions f_D. The increase of the deuterium fraction leads to a broadening of the infrared absorption band, due to the increased contribution of D_2O molecules for which the absorption spectrum of the O−D stretch vibration is substantially broader than for HDO.

Isotropic Transient Absorption. The left panel of Figure 3 shows difference spectra between the measured transient isotropic absorption spectra and the original absorption spectrum. The difference spectra show that the excitation by the pump pulse results in a decrease in absorption at frequencies near 2500 cm^{-1} due to the bleaching of the fundamental $v = 0 \rightarrow 1$ transition. Below 2420 cm^{-1} the signal

changes sign due to the induced $v = 1 \rightarrow 2$ absorption. With increasing delay time the transient signals decay and the bleaching signal shifts toward slightly higher frequencies. This finding indicates the presence of different water species showing different vibrational relaxation times. The spectral response at delay times >5 ps reflects an increase of the sample temperature that results after relaxation and thermalization of the excited O−D vibrations. An increase in sample temperature leads to a blue-shift of the fundamental absorption spectrum and a decrease of the absorption cross section. Hence, a rise in temperature leads to a bleaching (negative) signal at the red side of the transient difference spectrum (<2550 cm^{-1}) and an induced absorption (positive) signal at the blue side of this spectrum (>2550 cm^{-1}).

In Figure 4 we present the bleaching signal measured at 2500 cm^{-1} as a function of the delay between the pump and the
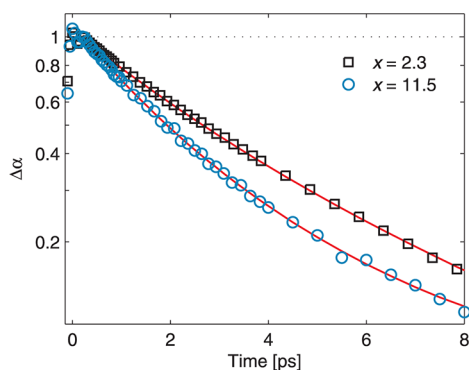
Figure 4. Transient absorption change at 2500 cm^{-1} as a function of delay between pump and probe for a deuterium fraction f_D of 0.25 and two different hydration levels.

probe for two different hydration levels and a deuterium fraction $f_D = 0.25$. The decay is clearly nonexponential for both hydration levels, showing the presence of different types of water with different vibrational relaxation time constants. The vibrational relaxation becomes faster with increasing degree of hydration.

For $f_D = 0.1$ and 0.25 we model the data with two types of HDO molecules that decay with different vibrational relaxation rates. The middle panel of Figure 3 shows the spectral components of these two types of HDO molecules. We attribute the faster species centered at 2470 cm^{-1} to HDO molecules being strongly hydrogen bonded to the phosphate

group of the lipids. The hydrogen bond between a water molecule and a carbonyl group is of very similar strength as the hydrogen bond between two water molecules. As a result, both water species absorb at the same frequency of 2500 cm^{-1}.[9] The slower component centered at that frequency is therefore assigned to HDO molecules that are hydrogen bonded to the carbonyl moieties and/or to other water molecules. This assignment is supported by molecular dynamics simulations.[12] The black spectrum represents the spectral change that results after full thermalization of the excitation energy.

In the left panel of Figure 5 we present the relative fractions of the fast and the slowly relaxing HDO molecules as a function of hydration level for $f_D = 0.1$. With increasing hydration level the relative amount of the fast HDO molecules decreases with respect to the slower species. The right panel of Figure 5 shows the vibrational lifetimes $T_{1,f}$ and $T_{1,s}$ of the two species as a function of hydration level (x). Both $T_{1,f}$ and $T_{1,s}$ decrease with increasing hydration level. The faster HDO molecules relax with $T_1 = 2.2 \pm 0.3$ ps at $x = 2.3$ and $T_1 = 1.2 \pm 0.1$ ps at $x = 11.5$. The slower HDO molecules decay with $T_1 = 5.6 \pm 0.4$ ps at $x = 2.3$ and $T_1 = 3.2 \pm 0.2$ ps at $x = 11.5$. Table 1 presents an overview of the fitted relaxation time constants for all measured deuterium fractions f_D and hydration levels x.

The amplitudes and vibrational lifetimes of the two species are in excellent, quantitative agreement with the results of recent molecular dynamics simulations by Gruenbaum et al.[12] The amplitudes and vibrational lifetimes extracted from their simulations are marked with asterisks in Figure 5. The experimental observations for $f_D = 0.1$ also agree with the results of recent work by Zhao et al. in which the vibrational dynamics of water molecules in hydrated DPLC membranes were studied at a deuterium fraction f_D of 0.05.[17] Similar observations were done for pure water hydrating DNA.[43,44] In these studies it was also observed that water molecules bound to the DNA backbone can be distinguished from the water molecules forming hydrogen bonds to other water molecules and that the vibrational relaxation rate increases with increasing hydration level,[43,44] exactly as we observe for hydrated DOPC membranes.

At a deuterium fraction f_D of 0.5, the hydration water not only consists of HDO but also comprises a significant amount of D_2O molecules (~25%). In modeling the data we describe the contribution of the D_2O molecules to the transient absorption as a third spectral component with an associated separate relaxation time constant. The time constants obtained from fitting the data at different hydration levels are presented
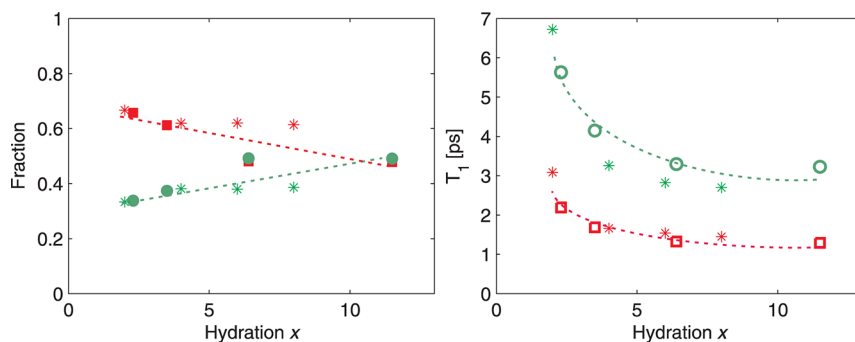
Figure 5. Relative fractions (left panel) and vibrational lifetimes (right panel) of the two different types of HDO molecules hydrating the DOPC bilayers as a function of hydration level, x. The fractions and vibrational lifetimes are obtained from a fit to the data obtained for a deuterium fraction f_D of 0.1. The asterisks represent the amplitudes and vibrational lifetimes resulting from the molecular dynamics simulations by Gruenbaum et al.[12]

Table 1. Relaxation Time Constants of the Different Spectral Components Resulting from the Fits of the Isotropic Data at All Studied Deuterium Fractions (f_D) and Hydration Levels (x)

| f_D | x | T_1 (ps) | | | τ_{therm} (ps) | τ_{cool} (ps) |
		HDO$_f$	HDO$_s$	D$_2$O		
0.1	2.3	2.2 ± 0.3	5.6 ± 0.4		−	−
	3.5	1.7 ± 0.2	4.1 ± 0.3	−	−	−
	6.4	1.3 ± 0.2	3.3 ± 0.3	−	−	−
	11.5	1.2 ± 0.1	3.2 ± 0.2	−	−	−
0.25	2.3	2.1 ± 0.2	5.5 ± 0.4	−	−	−
	3.5	1.7 ± 0.2	4.2 ± 0.3	−	−	−
	6.4	0.7 ± 0.1	2.7 ± 0.2	−	−	−
	11.5	0.6 ± 0.1	2.5 ± 0.2	−	−	−
0.5	2.3	2.1 ± 0.2	4 ± 0.3	0.6 ± 0.1	−	−
	3.5	1.6 ± 0.2	3.2 ± 0.3	0.5 ± 0.1	−	−
	6.4	1.4 ± 0.2	3 ± 0.3	0.35 ± 0.1	−	−
	11.5	0.8 ± 0.1	2 ± 0.3	0.25 ± 0.2	−	8.2 ± 2
1	2.3	−	−	0.4 ± 0.1	0.9 ± 0.2	2.4 ± 0.3
	3.5	−	−	0.4 ± 0.1	0.6 ± 0.1	2.5 ± 0.3
	6.4	−	−	0.4 ± 0.1	0.6 ± 0.1	4 ± 0.4
	11.5	−	−	0.4 ± 0.1	0.7 ± 0.1	6.3 ± 0.6
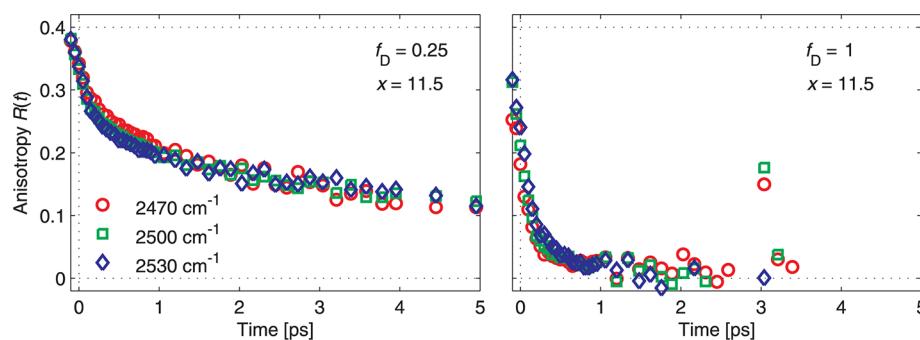
Figure 6. Anisotropy as a function of delay time measured at three different probe frequencies for water hydrating DOPC at a hydration level x of 11.5 and two different deuterium fractions f_D.

in Table 1. As was observed for the lower isotopic fractions, the vibrational lifetimes of all species decrease with increasing hydration level. The relaxation of all three components results in a local heating of the sample, as was also observed at low deuterium fractions. For $f_D = 0.5$ and $x = 11.5$, we observe a slow decay of the thermal signal with a time constant of ~8 ps. This decay is likely due to a cooling process in which the locally hot water transfers its excess thermal energy to the DOPC lipid layers.

For $f_D = 1$ there are only D$_2$O molecules present. We do not observe spectral or dynamical features that would allow us to disentangle D$_2$O molecules forming hydrogen bonds with the phosphate groups, carbonyl groups, or other water molecules. We model the relaxation of the D$_2$O molecules with a consecutive relaxation model that has been used before to describe the vibrational dynamics of bulk D$_2$O.[32] In this model the excited O−D stretch vibration first relaxes to a nonthermal intermediate state. This relaxation has a time constant T_1 of 0.4 ± 0.1 ps that is the same at all hydration levels. The nonthermal intermediate state subsequently relaxes with a thermalization time constant τ_{therm} of ~0.6 ps. This thermalization process involves the adaptation of the hydrogen bonds to the energy dumped by the vibrational relaxation of the O−D stretch vibrations and leads to the formation of a local hot state. Both the values of T_1 and τ_{therm} are similar to the relaxation time constants observed for pure D$_2$O.[32] The signal associated with

the local hot state shows a decay indicative of a cooling process (Table 1).

Anisotropy of the Transient Absorption. To determine the anisotropy of the O−D excitations, the measured $\Delta\alpha_\parallel(t)$ and $\Delta\alpha_\perp(t)$ of the excited O−D vibrations are first corrected for the ingrowing transient spectral response associated with the heating effect.[47] The thus corrected $\Delta\alpha_\parallel(t)$ and $\Delta\alpha_\perp(t)$ are used to construct the anisotropy using eq 11. In Figure 6 the anisotropy of the bleaching signal is presented as a function of the delay time for three different probe frequencies. The results show that the anisotropy dynamics are independent of the probe frequency.

In Figure 7 we present an overview of the anisotropy decay curves for all measured deuterium fractions and hydration levels. The anisotropy values are obtained by averaging the signals in a frequency window of 30 cm^{-1} around 2500 cm^{-1}. At all hydration levels x the anisotropy decays are strongly nonexponential. It is also seen that the anisotropy decay speeds up with increasing deuterium fraction f_D, which indicates the presence of resonant energy transfer. With increasing f_D the O−D oscillators located on different HDO and D$_2$O molecules will get closer, thus leading to a faster transfer of the excitation energy of an excited O−D vibration to a nonexcited O−D vibration. The results of Figure 7 also show that the starting value of the anisotropy decreases with increasing deuterium fraction f_D. This observation points to a rapid initial drop of the
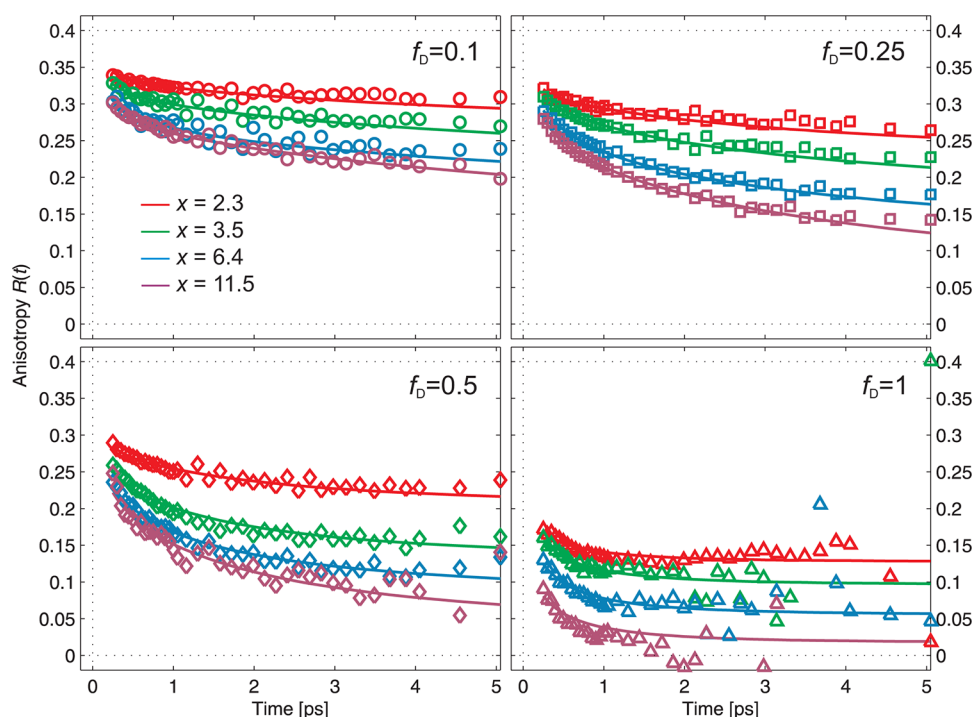
Figure 7. Anisotropy as a function of delay time for all studied hydration levels and deuterium fractions. The different hydration levels are indicated with different colors. The four panels represent data measured at the four studied deuterium fractions.

anisotropy as a result of fast intramolecular energy transfer within D_2O molecules. After ~3 ps, the anisotropy traces decay on such a slow time scale that they reach a constant end level within our experimental time window of 5 ps. The amplitude of this end level decreases with increasing hydration level x and deuterium fraction f_D.

The nonzero end values of the anisotropy curves of Figure 7 point at the presence of isolated water molecules that are at a too large distance from the other water molecules to show energy transfer within the experimental time window of 5 ps. These water molecules also show a low orientational mobility, at least for their O–D groups probed at 2500 cm^{-1}. In view of this probe frequency, these O–D groups are likely donating a hydrogen bond to the lipid and are "trapped" between closely residing lipid headgroups. It should be noted that the isolated water molecules can also contain a non-hydrogen bonded hydroxyl group that shows a much larger orientational mobility. However, these nonbonded O–D groups do not contribute to the signal because they absorb at a substantially higher frequency. The presence of isolated water molecules showing slow reorientation agrees with the results of molecular dynamics simulations by Bhide et al.[9,10] These slow water molecules were found to be located at the interface of the headgroup and tail, i.e., in the vicinity of the lipid carbonyl groups. The recent molecular dynamics simulations of Gruenbaum et al.[12] showed that the water molecules that are hydrogen bonded to the carbonyl groups possess the slowest orientational mobility of all water molecules adsorbed to the lipid membranes.

Modeling the Anisotropy Dynamics. The anisotropy dynamics shown in Figure 7 can be used to determine the distances between the water molecules hydrating the DOPC bilayers. This information is contained in the contribution of the intermolecular Förster energy transfer to the anisotropy dynamics. As the anisotropy is also affected by intramolecular

resonant energy transfer and molecular reorientation, we need to model the anisotropy dynamics taking into account all three contributions.

We consider a fraction of water molecules $A(x)$ showing both intermolecular energy transfer and orientational relaxation and a fraction of isolated water molecules $B(x)$ that shows neither energy transfer nor reorientation within the experimental time window. With increasing hydration level x the fraction $B(x)$ decreases, as expressed in the decrease of the end level of the anisotropy. Fractions $A(x)$ and $B(x)$ both contain a fraction of D_2O molecules (depending on the deuterium fraction f_D) that can show intramolecular energy transfer. We thus describe the anisotropy dynamics with the following expression:

$$R(f_D, x, t) = R_{IET}(f_D, x, t)\left[A(x)\, R_{Förster}(f_D, x, t)\right.$$
$$\left. R_{reo}(x, t) + B(x)\right] \tag{12}$$

$R_{IET}(f_D,x,t)$ is the initial drop of the anisotropy due to intramolecular energy transfer, $R_{Förster}(f_D,x,t)$ the decay due to intermolecular Förster energy transfer, and $R_{reo}(x,t)$ the anisotropy decay due to molecular reorientation.

For water molecules, intramolecular energy transfer is usually a very fast process[28−32] that does not lead to a full decay of the anisotropy because the excitation only becomes equilibrated over the plane of the water molecule.[48] We model the effect of intramolecular energy transfer as an instantaneous drop of the anisotropy of which the amplitude scales with the fraction of D_2O:

$$R_{IET}(f_D, x, t)$$
$$= \frac{S_{IET}(x)f_D{}^2 e^{-t/T_{1,D_2O}} + 2f_D(1 - f_D)e^{-t/T_{1,HDO}}}{f_D{}^2 e^{-t/T_{1,D_2O}} + 2f_D(1 - f_D)e^{-t/T_{1,HDO}}} \tag{13}$$

where f_D^2 is the fraction of D_2O molecules and $2f_D(1 - f_D)$ is the fraction of HDO molecules present. The amplitude $S_{IET}(x)$ represents the amplitude of the anisotropy that remains after intramolecular energy transfer within the D_2O molecules. The decrease in anisotropy due to intramolecular energy transfer only depends on the angle between the two O−D groups, even in case the vibrations would be best described as symmetric and asymmetric stretch vibrations. In the latter case, the angle between the two O−D groups determines the transition dipole moments of the two vibrations, and the decrease of the anisotropy due to intramolecular energy transfer depends on the relative magnitude of these transition dipole moments. The two O−D groups within the D_2O molecule have a relative angle of 104.5°, which implies that the intramolecular energy transfer leads to to a drop of the anisotropy to 0.297 times its initial value.[49] However, not all D_2O molecules will show rapid intramolecular energy transfer because the two O−D vibrations of the D_2O molecule can be far out of resonance, for instance when one of the O−D groups is hydrogen bonded to the lipid or to another water molecule while the other O−D is not hydrogen bonded. In that case there will be a large difference in vibrational frequency between the two O−D groups with the result that the intramolecular energy transfer will be very slow. Hence, the amplitude $S_{IET}(x) = 0.297f_{IET}(x) + (1 - f_{IET}(x))$, where $f_{IET}(x)$ is the fraction of the D_2O molecules showing rapid intramolecular energy transfer. The D_2O and HDO water molecules have different vibrational lifetimes that determine their visibility in the anisotropy. Therefore, the contributions of D_2O and HDO are weighted with their time-dependent excited populations. The vibrational lifetimes are extracted from the fits to the isotropic data.

We take the reorientation dynamics to be independent of the isotopic composition of the water molecules. Hence, the reorientation dynamics $R_{reo}(x,t)$ only depends on the hydration level x and not on the deuterium fraction f_D. We describe the reorientation as an exponential decay to a nonzero end level:

$$R_{reo}(x, t) = c(x)e^{-t/\tau_{or}(x)} + 1 - c(x) \tag{14}$$

where $\tau_{or}(x)$ is the reorientation time and $(1 - c(x))$ the end level. This modeling assumes that the reorientation shows a relatively fast component over a limited cone angle, leading to a partial decay of the anisotropy and a much slower component that hardly leads to a decay of the anisotropy within the experimental time window of 5 ps. These reorientation dynamics agree with the results of previous work.[9,10,12,17]

The intermolecular Förster vibrational energy transfer between the O−D groups located on different D_2O/HDO molecules is described using eq 9 of the theory section. In deriving eq 9 it is assumed that the spatial and orientation distribution of the acceptors is statistical and that the energy transfer is irreversible. In a recent theoretical study the validity of the Förster model has been discussed for resonant energy transfer in pure liquid water.[50] It was found that the nearest acceptors in liquid water are oriented such that the energy transfer leads to a negative anisotropy, thus making the observed anisotropy decay faster. On the other hand, the reversibility of the energy transfer leads to a slower decay of the anisotropy, and the two effects were found to compensate each other to a large extent.[50] We thus identify $R_{Förster}(f_D,x,t)$ with $\rho(t)$ of eq 9:

$$R_{Förster}(f_D, x, t) = \exp\left\{ -\frac{4\pi C_{OD}(f_D, x)a^3}{3} \exp\left(-\frac{tr_0^6}{T_1a^6}\right) \right.$$
$$\left. -\frac{4\pi^{3/2}C_{OD}(f_D, x)r_0^3\sqrt{t}}{3\sqrt{T_1}} \, \mathrm{erf}\left(\sqrt{\frac{tr_0^6}{T_1a^6}}\right) \right\} \tag{15}$$

By choosing the appropriate value of a, we can exclude the contribution of intramolecular energy transfer to $R_{Förster}$.

We performed a global fit of the 16 anisotropy curves of Figure 7 to eq 12. In this fit the parameter a is preset to $a = 1.8$ Å. This distance is larger than the intramolecular distance of the O−D groups in the D_2O molecule of ∼1.55 Å and shorter than the intermolecular distance, which is ∼2.2 Å. We verified that variation of a in between 1.6 and 2 Å has a negligible effect on the results of the fits. The Förster radius r_0 is a global fit parameter that is the same for all anisotropy curves. The values of $A(x)$, $B(x)$, and $f_{IET}(x)$ are the same at all isotopic compositions f_D, because the hydration structure is independent of the isotope composition. We also assume $c(x)$ and $\tau_{or}(x)$ to be independent of the isotope composition. Hence, all these parameters depend only on the hydration level x. The value of $C_{OD}(f_D,x)$ is expected to simply scale with the deuterium fraction f_D. Hence, as the other parameters only depend on the hydration level x, it is in principle possible to determine the concentrations C_{OD} at different hydration levels from a fit to the anisotropy curves measured at one particular value of the deuterium fraction f_D. However, at low f_D, the anisotropy dynamics on the picosecond time scale are dominated by the molecular reorientation, while at high f_D the anisotropy dynamics are dominated by intermolecular energy transfer. Hence, to obtain an accurate determination of both the molecular reorientation and the intermolecular energy transfer, we perform a global, simultaneous fit of the anisotropy curves measured at all four f_D values. In this global fit we treat the $C_{OD}(f_D,x)$ values at the different deuterium fractions and hydration levels as independent parameters for a consistency check. If the fit is consistent, the $C_{OD}(f_D,x)$ values resulting from the fit should scale with the deuterium fraction f_D.

Anisotropy Fit Results. The results of the global fit are represented by the solid lines in Figure 7. The molecular reorientation constitutes only a minor contribution to the decay of the anisotropy, as is directly evident from the limited decay of the anisotropy observed at a low deuterium fraction of $f_D = 0.1$. After 5 ps, the anisotropy decay due to reorientation ranges from 7% for $x = 2.3$ to 20% for $x = 11.5$. The coefficients $c(x)$ and time constants $\tau_{or}(x)$ resulting from the fit are presented in Table 2. The time constants $\tau_{or}(x)$ are in the range of 0.2−0.4 ps and probably reflect the librational motion of hydrogen bonded O−D groups that keeps the hydrogen bond intact. The librational motion takes place over a limited cone angle and

Table 2. Coefficients $[c(x)]$ and Time Constants $[\tau_{or}]$ Describing the Molecular Reorientation of the Hydration Water at Different Hydration Levels x

x	$c(x)$	τ_{or} (ps)
2.3	0.18 ± 0.03	0.2 ± 0.2
3.5	0.14 ± 0.03	0.3 ± 0.2
6.4	0.22 ± 0.03	0.4 ± 0.2
11.5	0.21 ± 0.03	0.3 ± 0.2
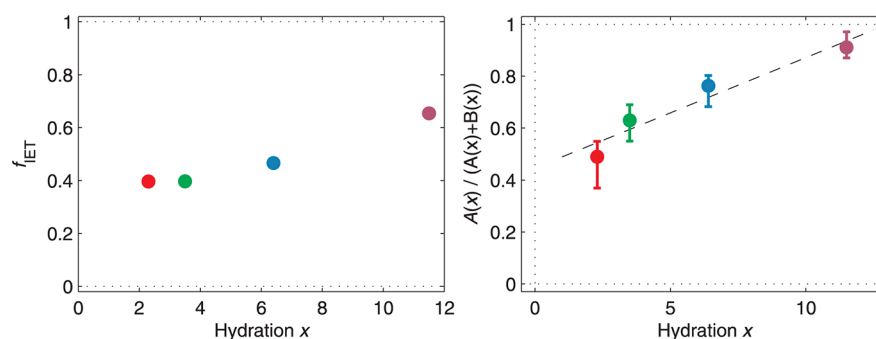
Figure 8. Left panel: fraction $f_{IET}(x)$ of the D_2O molecules that show rapid intramolecular energy transfer and thus contribute to the fast initial drop of the anisotropy of the O–D excitation. Right panel: fraction $A(x)$ of water molecules showing resonant intermolecular Förster vibrational energy transfer.
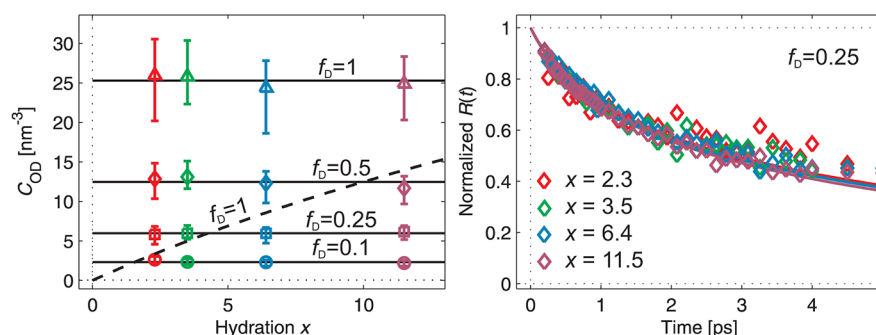
Figure 9. Left panel: the concentration $C_{OD}(f_D,x)$ of O–D oscillators showing Förster vibrational energy transfer as a function of the hydration level x, for all four measured deuterium fractions f_D. The left panel also shows the value of $C_{OD,hom}(f_D=1,x)$ that corresponds to a completely homogeneous distribution of the O–D oscillators over the lipid membranes (dashed curve). Right panel: normalized anisotropy decays due to intermolecular energy transfer at different hydration levels for $f_D = 0.25$.

thus only leads to a small partial decay of the anisotropy. The time scale of this motion is similar to what has been observed for the librational motion of hydroxyl groups in neat liquid water.[51]

The intramolecular energy transfer leads to an initial drop of the anisotropy, the magnitude of which depends the fraction $f_{IET}(x)$ of the D_2O molecules that show rapid intramolecular energy transfer. In the left panel of Figure 8 the fraction $f_{IET}(x)$ is presented as a function of the hydration level x. For all hydration levels, $f_{IET}(x)$ is substantially lower than 1, showing that for many D_2O molecules the O–D groups are out of resonance with each other, which indicates that for these D_2O molecules only one of the O–D groups is hydrogen bonded.

The intermolecular Förster energy transfer dominates the anisotropy dynamics on the picosecond time scale for deuterium fractions $f_D \geq 0.25$. From the fit we obtain a Förster radius r_0 of 2.4 ± 0.2 Å, which is a measure of the coupling strength of the O–D oscillators. The Förster radius of 2.4 ± 0.2 Å is very similar to the value of 2.3 Å found for the Förster energy transfer between the O–D vibrations in D_2O/H_2O mixtures.[32] The fact that the value of r_0 of 2.4 ± 0.2 Å is quite similar to that of O–D vibrations in neat liquid water shows that the intrinsic inhomogeneity of the water molecules hydrating the DOPC lipids does not lead to a decrease of the rate of intermolecular Förster energy transfer. The water molecules hydrogen bonded to phosphate apparently still show good spectral overlap with the water molecules that are hydrogen bonded to carbonyl groups or to other water molecules. This finding can be explained by the fact that the central frequency of these water molecules only differs by 30

cm^{-1}, which is small in comparison to the homogeneous line width of the O–D stretch vibration that will be on the order of 100 cm^{-1}.[53] In addition, the decrease in Förster coupling due to the somewhat poorer spectral overlap can be compensated by the larger transition dipole moment of the O–D vibrations that are strongly hydrogen bonded to the phosphate groups.

In the right panel of Figure 8 we show the fractions $A(x)$ (water molecules involved in intermolecular Förster energy transfer) and $B(x)$ (isolated water molecules) resulting from the fit. We find that $A(x)$ increases from 0.47 ± 0.04 for $x = 2.3$ to 0.93 ± 0.04 for $x = 11.5$. We thus find that at a low hydration level $x = 2.3$, approximately 45% of the water molecules are showing Förster energy transfer. This is a relatively high value in view of the fact that there are ~2 water molecules per lipid. Due to the r^{-6} dependence of the transfer rate, these water molecules need to reside rather close to each other to exhibit a (sub)picosecond Förster energy transfer time, which implies that a large part of the water molecules forms clusters already at low hydration levels. With increasing hydration level, the fraction $A(x)$ increases, and at a hydration level of ~12 water molecules per lipid (which is the maximal amount of water molecules a DOPC molecule can coordinate[52]), nearly all water molecules are involved in the Förster energy transfer, meaning that almost all water molecules will be contained in clusters. However, even at this highest hydration level the fraction $B(x)$ does not vanish completely, meaning that there are still water molecules that are sufficiently isolated from the rest to be excluded from Förster energy transfer.

In the left panel of Figure 9 we present the values of $C_{OD}(f_D,x)$ resulting from the fit as a function of the hydration

level. It is seen that the obtained $C_{OD}(f_D,x)$ values scale with the value of f_D, illustrating that the global fit of the anisotropy curves to eq 12 provides a consistent description of the dynamics at all studied deuterium fractions. In this figure, we also show the value of $C_{OD,hom}(f_D=1,x)$ that would be observed in case the water molecules were homogeneously distributed over the lipid layers (dashed line). The concentration $C_{OD,hom}(f_D=1,x)$ is given by

$$C_{OD,hom}(f_D=1, x) = \frac{2x}{V_{DOPC} + V_{D_2O}x} \qquad (16)$$

where x is the hydration number, V_{DOPC} is the volume of a DOPC molecule, and V_{D_2O} is the volume of a D_2O molecule. The volume of a DOPC molecule amounts to $\sim$1300 Å^3.[54,55] The volume of a D_2O molecule is $\sim$30 Å^3. Clearly at all hydration levels, the homogeneous $C_{OD,hom}(f_D=1,x)$ is much lower than the observed $C_{OD}(f_D=1,x)$, which implies that the water molecules strongly cluster, even at low hydration levels.

DISCUSSION

At $f_D = 1$, we find a value for C_{OD} of 25 ± 2 nm^{-3} for all hydration levels x, which corresponds to an average intermolecular distance of the water molecules showing Förster energy transfer of 3.4 Å. In the case of a homogeneous distribution of water molecules over the membrane, the average distance would have varied from 7 Å for $x = 2.3$ to 4.2 Å for $x = 11.5$. For pure D_2O, $C_{OD} = 66$ nm^{-3}, corresponding to an average distance between the O–D groups of 2.5 Å. Hence, the average distance of 3.4 Å in the water clusters is significantly smaller than the intermolecular distance in the case where the water molecules would have been homogeneously distributed over the lipid layers but larger than the average distance in liquid water. The larger average distance between the water molecules in the clusters likely results from the lipid headgroup moieties protruding into the clusters, thereby diluting somewhat the water content of the cluster. This finding indicates that the clusters are not spherical in shape and possibly form elongated structures along the phosphate, carbonyl, and choline groups.

An important result is that the concentration $C_{OD}(f_D,x)$ shows very little dependence on the hydration level x (Figure 9). To further illustrate this finding, we show in the right panel of Figure 9 the normalized anisotropy decay of the $A(x)$ water fraction for different hydration levels for $f_D = 0.25$. These decays are obtained by subtracting the $B(x)$ fraction and the contributions of the molecular reorientation and the intramolecular energy transfer. Hence, these decays only present the anisotropy decay due to intermolecular Förster energy transfer. It is seen that within the error margins these decays are the same for all studied hydration levels. The observed changes in anisotropy dynamics in Figure 7 with increasing hydration level thus primarily result from the increase of the fraction $A(x)$.

The independence of $C_{OD}(f_D,x)$ on the hydration level shows that the water molecules hydrating the membrane are contained in clusters whose shape and size remain similar when the hydration is increased up to a hydration level of $x = 12$. It should be noted here that the studied hydration levels are rather low in comparison to physiological conditions, in which lipid bilayers are usually separated by a thick layer of water.[56] In an X-ray diffraction study of DOPC membranes it was found that the slope of the Bragg spacing as a function of hydration level shows a sharp increase at $x = \sim$12. This result indicates

that the hydration water changes in character at hydration levels $x > 12$, which may point at the formation of a connected water network at these higher hydration levels. The formation of a connected water network at higher hydration levels is supported by recent molecular dynamics simulations that showed the presence of such a water network for DLPC membranes at a hydration level of $x = 16$.[12]

CONCLUSIONS

We measured the energy relaxation and anisotropy dynamics of the O–D stretch vibrations of HDO and D_2O molecules hydrating DOPC membranes with polarization-resolved femtosecond mid-infrared pump–probe spectroscopy. In the experiments we varied the hydration level x from 2 to 12 water molecules per DOPC lipid, and we varied the deuterium fraction f_D from 0.1 to 1.

The transient absorption data at low deuterium fractions reveal the presence of two water species. We attribute the species centered at 2470 cm^{-1} to HDO molecules being strongly hydrogen bonded to the phosphate group of the lipids. The species centered at 2500 cm^{-1} can be assigned to HDO molecules that are hydrogen bonded to the carbonyl moieties and to other water molecules.

The anisotropy dynamics at a low deuterium fraction $f_D = 0.1$ show that the molecular reorientation consists of a relatively small fast component ($\sim$20%) and a large slow component that does not lead to a significant decay of the anisotropy within the experimental time window of 5 ps. The fast component is likely associated with the librational motion of hydrogen bonded hydroxyl groups that keeps the hydrogen bond to the lipid headgroup intact.

The anisotropy shows a significant acceleration with increasing deuterium fraction f_D, showing the occurrence of resonant (Förster) energy transfer between the hydrating HDO and D_2O molecules. We analyze the data with a novel expression (eq 9) for the Förster vibrational energy transfer that excludes the contribution of intramolecular energy transfer events between the two O–D groups of a D_2O molecule. Hence, eq 9 exclusively accounts for the intermolecular energy transfer events. We find that water hydrating DOPC membranes forms nanoclusters already at low hydration levels with an average intermolecular distance of 3.4 Å. This value does not change when the hydration level is increased, which indicates that the size and shape of the clusters do not significantly change. Only the density of the clusters increases with increasing hydration level.

The present results demonstrate that the measurement of the rate of intermolecular Förster energy transfer forms a very effective tool to determine the distribution of water molecules hydrating a surface or a large (bio)molecular system. The method requires the measurement of the anisotropy dynamics of the hydroxyl stretch vibrations of water with polarization-resolved femtosecond spectroscopy and can in principle be applied to any hydrated system. The method works best with water of intermediate isotopic composition, e.g., D_2O:H_2O = 25:75 or 50:50, because for these mixtures the anisotropy dynamics is not dominated by intramolecular energy transfer (as is the case for pure D_2O), and the intermolecular energy transfer between the O–D vibrations is sufficiently fast to be measured within the vibrational lifetime.

■ AUTHOR INFORMATION

Corresponding Author
*E-mail: lukasz.piatkowski@icfo.es.

Notes
The authors declare no competing financial interest.

■ REFERENCES

(1) Lee, A. G. *Biochim. Biophys. Acta* **2004**, *1666*, 62−87.
(2) Volke, F.; Eisenblatter, S.; Galle, J.; Klose, G. *Chem. Phys. Lipids* **1994**, *70*, 121−131.
(3) Wassall, S. R. *Biophys. J.* **1996**, *71*, 2724−2732.
(4) Nilsson, A.; Holmgren, A.; Lindblom, G. *Biochemistry* **1991**, *30*, 2126−2133.
(5) Binder, H.; Pohle, W. *J. Phys. Chem. B* **2000**, *104*, 12039−12048.
(6) Binder, H. *Eur. Biophys. J.* **2007**, *36*, 265−279.
(7) Gouliaev, N.; Nagle, J. F. *Phys. Rev. Lett.* **1998**, *81*, 2610−2613.
(8) Lopez, C. F.; Nielsen, S. O.; Klein, M. L.; Moore, P. B. *J. Phys. Chem. B* **2004**, *108*, 6603−6610.
(9) Bhide, S. Y.; Berkowitz, M. L. *J. Chem. Phys.* **2005**, *123*, 224702.
(10) Bhide, S. Y.; Berkowitz, M. L. *J. Chem. Phys.* **2006**, *125*, 094713.
(11) Zhang, Y.; Fujisaki, H.; Straub, J. E. *J. Phys. Chem. A* **2009**, *113*, 3051−3060.
(12) Gruenbaum, S. M.; Skinner, J. L. *J. Chem. Phys.* **2011**, *135*, 075101.
(13) Cheng, J.-X.; Pautot, S.; Weitz, D. A.; Xie, X. S. *Proc. Natl. Acad. Sci. U. S. A.* **2003**, *100*, 9826−9830.
(14) Volkov, V. V.; Nuti, F.; Takaoka, Y.; Chelli, R.; Papini, A. M.; Righini, R. *J. Am. Chem. Soc.* **2006**, *128*, 969−982.
(15) Volkov, V. V.; Palmer, D. J.; Righini, R. *J. Phys. Chem. B* **2007**, *111*, 1377.
(16) Victor, V. V.; Palmer, D. J.; Righini, R. *Phys. Rev. Lett.* **2007**, *99*, 078302.
(17) Zhao, W.; Moilanen, D. E.; Fenn, E. E.; Fayer, M. *J. Am. Chem. Soc.* **2008**, *130*, 13927−13937.
(18) Volkov, V. V.; Takaoka, Y.; Righini, R. *J. Phys. Chem B* **2009**, *113*, 4119−4124.
(19) Sovago, M.; Vartiainen, E.; Bonn, M. *J. Chem. Phys.* **2009**, *131*, 161107.
(20) Ghosh, A.; Campen, R. K.; Sovago, M.; Bonn, M. *Faraday Discuss.* **2009**, *141*, 145−159.
(21) Bonn, M.; Bakker, H. J.; Ghosh, A.; Yamamoto, S.; Sovago, M.; Campen, R. K. *J. Am. Chem. Soc.* **2010**, *132*, 14971−14978.
(22) Klösgen, B.; Reichle, C.; Kohlsmann, S.; Kramer, K. D. *Biophys. J.* **1996**, *71*, 3251−3260.
(23) Tielrooij, K. J.; Paparo, D.; Piatkowski, L.; Bakker, H. J.; Bonn, M. *Biophys. J.* **2009**, *97*, 2484−2492.
(24) Rehm, D.; Eisenthal, K. B. *Chem. Phys. Lett.* **1971**, *9*, 387−389.
(25) Gochanour, C. R.; Andersen, H. C.; Fayer, M. D. *J. Chem. Phys.* **1979**, *70*, 4254−4271.
(26) Fleming, G. R.; Scholes, G. D. *Nature* **2004**, *431*, 256−257.
(27) McArthur, E. A.; Eisenthal, K. B. *J. Am. Chem. Soc.* **2006**, *128*, 1068−1069.
(28) Woutersen, S.; Bakker, H. J. *Nature* **1999**, *402*, 507−509.
(29) Cowan, M. L.; Bruner, B. D.; Huse, N.; Dwyer, J. R.; Chugh, B.; Nibbering, E. T. J.; Elsaesser, T.; Miller, R. J. D. *Nature* **2005**, *434*, 199−202.
(30) Kraemer, D.; Cowan, M. L.; Paarmann, A.; Huse, N.; Nibbering, E. T. J.; Elsaesser, T.; Miller, R. J. D. *Proc. Natl. Acad. Sci. U. S. A.* **2008**, *105*, 437−442.
(31) Paarmann, A.; Hayashi, T.; Mukamel, S.; Miller, R. J. D. *J. Chem. Phys.* **2008**, *128*, 191103.

(32) Piatkowski, L.; Eisenthal, K. B.; Bakker, H. *J. Phys. Chem. Chem. Phys.* **2009**, *11*, 9033−9038.
(33) Förster, T. F. *Z. Naturforschg* **1940**, *4*, 821−827.
(34) Asher, S. A.; Pershan, P. S. *Biophys. J.* **1979**, *27*, 393−421.
(35) Hristova, K.; White, S. H. *Biophys. J.* **1998**, *74*, 2419−2433.
(36) Hallock, K. J.; Wildman, K. H.; Lee, D. K.; Ramamoorthy, A. *Biophys. J.* **2002**, *82*, 2499−2503.
(37) Tristram-Nagle, S. A.; Nagle, J. F. *Chem. Phys. Lipids* **2004**, *127*, 3−14.
(38) Tristram-Nagle, S. A. *Methods Mol. Biol.* **2007**, *400*, 63−75.
(39) Levine, Y. K.; Bailey, A. I.; Wilkins, M. H. *Nature* **1968**, *220*, 577−578.
(40) Levine, Y. K.; Wilkins, M. H. *Nat. New Biol.* **1971**, *230*, 69−72.
(41) Wiener, M. C.; King, G.; White, S. H. *Biophys. J.* **1991**, *60*, 568−576.
(42) Wiener, M. C.; White, S. H. *Biophys. J.* **1992**, *62*, 434−447.
(43) Szyc, L.; Dwyer, J. R.; Nibbering, E. T. J.; Elsaesser, T. *Chem. Phys. Lett.* **2009**, *357*, 36−44.
(44) Szyc, L.; Yang, M.; Nibbering, E. T. J.; Elsaesser, T. *Angew Chem Int. Ed* **2010**, *49*, 3598−3610.
(45) Beranová, L.; Humpoličková, J.; Sýkora, J.; Benda, A.; Cwiklik, L.; Jurkiewicz, P.; Gröbner, G.; Hof, M. *Phys. Chem. Chem. Phys.* **2012**, *14*, 14516−14522.
(46) Róg, T.; Murzyn, K.; Milhaud, K.; Karttunen, M.; Pasenkiewicz-Gierula, M. *J. Phys. Chem. B* **2009**, *113*, 2378−2387.
(47) Rezus, Y. L. A.; Bakker, H. J. *J. Chem. Phys.* **2005**, *123*, 114502.
(48) Cringus, D.; Jansen, T. C.; Pshenichnikov, M. S.; Wiersma, D. A. *J. Chem. Phys.* **2007**, *127*, 084507.
(49) Lipari, G.; Szabo, A. *Biophys. J.* **1980**, *30*, 489−506.
(50) Yang, M.; Li, F.; Skinner, J. L. *J. Chem. Phys.* **2011**, *135*, 164505.
(51) Fecko, C. J.; Loparo, J. J.; Roberts, S. T.; Tokmakoff, A. *J. Chem. Phys.* **2005**, *122*, 054506.
(52) Jendrasiak, G. L.; Smith, R. L. *Chem. Phys. Lipids* **2004**, *131*, 183−195.
(53) Steinel, T.; Asbury, J. B.; Corcelli, S. A.; Lawrence, C. P.; Skinner, J. L.; Fayer, M. D. *Chem. Phys. Lett.* **2004**, *386*, 295−300.
(54) Greenwood, A. I.; Tristram-Nagle, S.; Nagle, J. F. *Chem. Phys. Lipids* **2006**, *143*, 1−10.
(55) White, S. H.; Jacobs, R. E.; King, G. I. *Biophys. J.* **1987**, *52*, 663−665.
(56) Parry, J. M.; Hagen, M.; Mouritsen, O. G.; Kinnunen, P. K. J.; Alakoskela, J.-M. I. *Langmuir* **2010**, *26* (7), 4909−4915.